sciendo

Archives of Hydro-Engineering and Environmental Mechanics
Vol. 67 (2020), No. 1–4, pp. 35–53
DOI: 10.1515/heem-2020-0003
ISSN 1231–3726

Modelling of Quadratic-Surface Sludge Digesters by Smoothed Particle Hydrodynamics (SPH) – Finite Element (FE) Methods

Kiran Tota-Maharaj[1], Ghassan Nounu[2], Navin Ramroop[3]

[1]Aston University Birmingham, Department of Civil Engineering, School of Infrastructure and Sustainable Engineering, Birmingham, B4 7ET, U.K., e-mail: k.tota-maharaj@aston.ac.uk, [2]University of the West of England, Civil and Environmental Engineering Cluster, Faculty of Environment and Technology, Coldharbour Ln, Stoke Gifford, Bristol BS16 1QY, U.K., e-mail: Ghassan.Nounu@uwe.ac.uk, [3]The University of Trinidad and Tobago, Centre for Project Management and Civil Infrastructure Systems, San Fernando Campus, Tarouba Link Road, San Fernando, Trinidad. W.I., e-mail: Navin.Ramroop@utt.edu.tt

(Received April 11, 2020; revised December 07, 2020)

Abstract

The quadric-surfaced sludge digester (QSD), also known as the egg-shaped sludge digester, has proven its advantages over traditional cylindrical digesters recently. A reduction in operational cost is the dominant factor. Its shell can be described as a revolution of a parabola with the apex and base being either tapered or spherical. This shape provides a surface free of discontinuities, which is advantageous regarding the efficiency during mixing. Since the shape does not produce areas of inactive fluid motion within the tank, sludge settlement and an eventual grit build-up are avoided. The stresses developed in the shell of the sludge digester, vary along the meridian and equatorial diameters. A non-dimensional parameter, ξ, defines the height-to-diameter aspect ratio which is used to delineate the parametric boundary conditions of the shell's surface. Three groups of analyses were conducted to determine the orthogonal stresses in the shell of the QSD. The first-principles numerical models ran reasonably quickly, and many simulations were made during the study. The results showed that they were in within the range 5.34% to 7.2% to 2D FEA results. The 3D FEA simulation results were within the range of 8.3% to 9.2% to those from the MATLAB time-history models. This is a good indicator that the first principles numerical models are an excellent time-saving method to predict the behaviour of the QSD under seismic excitation. Upon examining the criteria for the design, analysing the results for the 2D FEA simulations showed that the fill height is not a significant variable with sloshing however the 3D FEA showed that the hydrostatic pressure is a significant variable. With the maximum tensile stress of the 3D-printed Acrylonitrile Butadiene Styrene (ABS)-a common thermoplastic polymer typically used for injection molding applications, being 24.4 MPa, the overall maximum stress of 5.45 MPa, the material can be a viable option for the use of QSD construction in small island developing states (SIDS).

Key words: hydraulic infrastructure, Egg-shaped reactors, quadric-surfaced sludge digesters, shell structures, Small Island Developing States (SIDS)

1. Introduction

Traditionally, domestic wastewater across small island developing states (SIDS), have been treated via localised septic tanks. In much low-income residential and rural communities, pit latrines are still being utilised. Climatic changes have redistributed rainfall intensities causing smaller islands to look closer at water quantities accounting and the reuse of wastewater with the appropriate infrastructure may now become essential in areas where low supplies of potable water continue to impact the wider communities. There is a degree difficulty for assessing proper functionality of these structures since little or no maintenance usually occurs during the life of these hydraulic structures. Hence, groundwater contamination in the indigenous aquifers becomes a high possibility. Centralised wastewater treatment facilities can eliminate groundwater contamination hence not only ensuring the non-pollution of groundwater but also providing reuse of treated water for commercial activities. Some SIDS are heavily dependent on tourism and are reliant on using water for activities such as landscaping (Hutchinson 2010). Wastewater reuse can be a supplemental alternative for water resources when compared to the reliability of rainwater harvesting. The secondary treatment phase offers removal of bacteria and sludge from the effluent, preparing it for the final or tertiary stage of disinfection. Within the secondary treatment stage, anaerobic digestion of the sludge usually takes place in a sludge digester. These tanks are typically cylindrical. The problem with this shape is that due to improper mixing, dead zones (see Figure 1) develop, leaving a build-up of scum and grit on the tank walls (Zingoni 2001). The question arises how one can construct or fabricate a 25-metre hydraulic structure with 3-D printing. The research carried out in this study looks at the feasibility of 3-D printing several major components of an egg-shaped sludge digester and assembled later on at various locations. This can result in the stresses concentrated at certain points such as connecters and joints across the 3-D printed assembled hydraulic structure.

This inefficiency causes the plant operations to be temporarily halted to facilitate cleaning of these sludge digesters. Recommencing operation of the tanks usually requires time and energy for the bacteria to develop which results in further delays. With the advent of the quadric surfaced sludge digester, the efficiency of mixing is increased, thus eliminating the scum build-up, hence reducing the overall costs associated with operation and maintenance. The quadric-surfaced sludge digester (QSD) has seen few iterations in design since its initial development. Although the benefit of lower maintenance cost outweighs the initial cost of construction, this has not been an attractive reason for adoption in Caribbean small island developing states (SIDS). It is due to the lack of construction expertise and procurement of special purpose-made formwork and other equipment that comes at a high cost. A reduction in this cost can provide a means for SIDS to adopt the QSD for integration in their wastewater treatment facilities. Replacing the primary material with a 3D printed polymer can provide rapid off-site production of the QSD in a modular manner, which can be shipped and

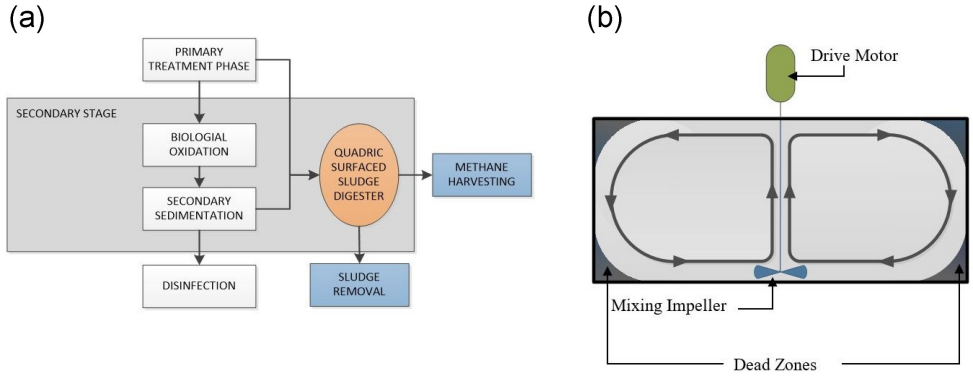

Fig. 1. (a) Schematic of the secondary treatment process in Wastewater Treatment Works, (b) Mixing pattern in a typical cylindrical digester showing dead zones

assembled on-site with semi-skilled labour. This research examines the possibility of using Acrylonitrile Butadiene Styrene (ABS) as the primary material and 3D fused deposition manufacturing as the main construction method. This study conducts various numerical analyses to determine the applicability of using 3D printed ABS for QSDs under seismic loads. The analyses conducted measured the load effects of hydrostatic and dynamic pressures on different height-to-diameter ratios of a parabolic ogival form for the QSD. In this research project various numerical methods were examined to calculate the stresses developed in QSD structure walls, depending on the water levels within the tank and characteristics of the driving forces.

1.1. Sloshing Dynamics

Sloshing is of significant importance in hydraulic wastewater infrastructure and is one of the major concerns in the design of liquid retaining structures and fuel tankers for carriers. Abramson (1967), stated that for several years, this subject has been a major concern for engineers, scientists, mathematicians and practitioners. According to Ibrahim (2006),the free liquid's surface can experience different motions comprising of simple planar, non-planar, symmetric, asymmetric, rotational, irregular beating, quasi-periodic and chaotic, all depending on the type of disturbance, amplitude and frequency of seismic excitation, properties of the liquid, height of liquid and the geometry of the retaining liquid container. Sumner (1966) defined Stable Nonplanar Motion as a steady-state rotary motion of a liquid surface with constant wave height peaks and a single nodal diameter, which rotates in one direction at a constant angular velocity, whereby the frequency of the angular rotation of the nodal diameter is equal to the excitation frequency of the tank (Sumner 1966). Unstable nonplanar motion is a rotary motion of the liquid surface that never attains a steady-state harmonic response; that is, the (i) peak wave height and (ii) nodal diameter rate and direction of-rotation continually change with time (Sumner 1966). When the frequency of the

motion and the natural frequencies of liquid sloshing are close to each other, the resulting amplitudes of the sloshing wave would be very large increasing the sloshing dynamic forces on the shell surfaces of the container. The high hydrodynamic forces produced by the sloshing waves on the inner surface of the container affects the overall response of the container and causes a complex Fluid–Structure Interaction (FSI) phenomenon between the two materials with respect to the liquid properties and retaining container properties. The linear theory of dynamic sloshing in liquid retaining structures is based on understanding the derivation of fluid field equations that are used to approximate the hydrodynamic shell forces and moments induced by sloshing waves. Ibrahim (2006), mentioned that the linear theory for liquid sloshing is acceptable for determining the natural frequencies and wave height of the liquid's free surface. Under translational excitation, the linear theory is useful for predicting the shell's liquid hydrodynamic pressure, forces, and moments. Only applicable when the free surface maintains a planar shape with a nodal diameter that remains perpendicular to the line of excitation, and it does not take into consideration the importance of vertical displacement with respect to the centre of gravity of the liquid for large amplitudes of sloshing.

Furthermore, Ibrahim (2006) found that the linear theory fails to predict complex surface phenomena observed experimentally near resonance. These phenomena include the non-planar unstable motion of the liquid's free surface associated with chaotic sloshing and rotation of the nodal diameter also called rotary sloshing. He also states that the linear theory cannot be used for dynamic analysis of shell elements undergoing elastic deformation that is analogous to its wall thickness and also if the liquid's free surface amplitude is large. The shell structure kinematics and deformation can be a finite elastic or finite plastic strains, based through a transverse normal material fibre, being stretched and bended as well as shear deformations. Nonlinear resonance conditions that cause complex response characteristics will result in the occurrence of nonlinearities within a Finite Element Analysis (FEA) model.

The method being utilised in analysing fluid-structure complications of this investigation is called the Smooth Particle Hydrodynamics (SPH) method which is a meshless Lagrangian procedure used to model the liquid conditions under applied motion. In this method, the fluid region is represented by particles, which convey information about mass conservation, hydrodynamic and thermodynamic performance. Since this is a meshless technique, problems that involve large-amplitude fluid motion and complex geometries can be solved very easily producing more accurate results as opposed to the grid numerical methods mentioned in the previous section, without having the limitations of volumetric meshing. This method is computationally expensive with respect to both memory and CPU time because analysis requires a large number of particles to simulate the actual phenomena of FSI problems. The more particles modelled the result accuracy will increase. This method will be adopted as one of the methods for numerical analysis to investigate dynamic sloshing of the QSD. The SPH procedure can understand hydrodynamics intricacies whose arrangement appear as

a PDE for field factors such as the density, velocity and energy. Acquiring expository solutions for such an arrangement of PDEs is not frequently conceivable, aside from not very many straightforward cases. For numerical arrangements, one needs first to discretize the problem area where the PDEs are characterised so that the technique can give an estimate to the estimations of the field capacities and their derivatives at any point.

1.2. Seismicity of the Caribbean Region

Extensive diversity of tectonic regimes characterizes the perimeter of the Caribbean plate, involving no fewer than four major adjacent plates (North American, South American, Nazca, and Cocos). Inclined zones of deep earthquakes, deep ocean trenches, and arcs of volcanoes clearly indicate subduction of oceanic lithosphere along the Central American and Atlantic Ocean boundaries of the Caribbean plate, while shallow seismicity and focal mechanisms of significant shocks in Guatemala, northern Venezuela, and the Cayman Ridge and Cayman Trench indicate a transform fault and divergent basin tectonics. The depth profile panels portray earthquakes that extend from the Middle America Trench axis in the west to depths as much as 300 km beneath Guatemala and from the Lesser Antilles Trench axis in the East to depths close to 200 km beneath Guadeloupe and the northeast Caribbean. In contrast, seismicity along the portions of the Caribbean plate margins from Guatemala to Hispaniola and from Trinidad to western Venezuela is suggestive of transform fault tectonics. Along the northern margin of the Caribbean Plate, the North America plate moves west, relative to the Caribbean plate, at approximately 20 mm/year, resulting in major trans-current faults and troughs. Further east, the North America plate subducts the Caribbean plate which results in surface expression of the deep Puerto Rico Trench. Hence, a zone of intermediate focus earthquakes develops in the subducted slab. The plate boundary curves around Puerto Rico and the northern portion of the Lesser Antilles where the plate motion vector of the Caribbean plate relative to the North and South American plates is less oblique, resulting in active island-arc tectonics. The North and South America plates subduct the Caribbean plate along the Lesser Antilles Trench at rates of about 20 mm/year; consequently, there are both intermediate focus earthquakes within the subducted South America plate and an array of active volcanoes along the archipelago. The southern Caribbean plate boundary along with the South America plate strikes in an east-west direction across the island of Trinidad and western Venezuela and is characterised by significant strike-slip faults and shallow seismicity, resulting from relative plate movement of about 20 mm/year. Further to the west, a broad zone of convergence moves southwest to western Venezuela and central Columbia. Plate boundaries transition from Caribbean/South America convergence in the east to Nazca/South America convergence in the west. The Nazca-Caribbean plate boundary offshore of Columbia is differentiated by convergence at about 65 mm/year. The Cocos plate, along the western coast of Central America, subducts the

Caribbean plate at rates of 72–81 mm/year, resulting in a relatively high seismic hazard and a chain of numerous active volcanoes; here intermediate-focus earthquakes occur within the subducted zone of the Cocos plate to depths of nearly 300 km. The time history acceleration records used for this research are from Japan. Japan was chosen because it shares seismic similarities with the Caribbean. These include:

- Located within a subduction zone,
- Characterised predominantly by shallow seismicity.

The primary mechanism for earthquakes in both countries are the reverse fault due to the convergent plate boundary at the subduction zone; and the strike-slip which occurs parallel to the direction of subduction (plate motion). The time history records were retrieved from PEER-NGA-West2 database. The NGA-West2 consists of an extensive, comprehensive set of time history recorded worldwide in active tectonic regimes. The earthquake used for this investigation was the Great Hanshin earthquake or the Kobe earthquake which occurred in Japan on January 17, 1995 and is referenced: Kobe; RSN 1120; Takatori 1995 as shown in Table 1.

Table 1. Earthquake parameters from Kobe;RSN 1120; Takatori 1995 used in the simulation

Earthquake Parameter	**Ground Motion Information**
The National Geospatial-Intelligence Agency (NGA) Record Sequence Number	1120
Magnitude (Moment Magnitude Scale)	6.9
Closest Distance	1.5 km
Hypocentral Distance	22.19 km
Velocity	256 m/s
Mechanism	Strike Slip
Period-Peak (T_p)	1.55 seconds
Peak Ground Velocity (PGV)	153.2 cm/s

For this study, typical magnitudes of earthquakes occurring in the Caribbean are far less than 7.0 on the moment magnitude scale, hence the use of such a magnitude in relation to the ground accelerations are necessary in designing and construction critical infrastructure in determining the forces acting the wastewater structure (QSD) under investigation.

2. Numerical Modelling of Quadric-Surfaced Sludge Digesters (QSDs)

2.1. First Principles Model

The first principles models examined the QSDs under various loading parameters. A digester of 25 m height and wall thickness of 500mm was modelled and analysed with varying fill levels of 10%, 25%, 50%, 75% and 90%. All models were each categorised based on the dimensions, as shown in Figure 2. The second group of analyses are a series of 2D FEA models, and finally a 3D FEA model was analysed.

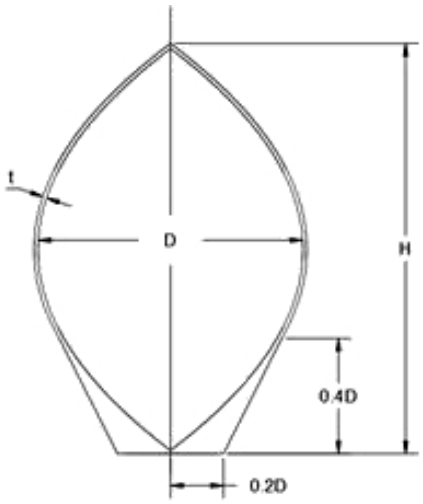

Fig. 2. Quadric-Surfaced Sludge Digesters (QSD) dimensions

When a horizontal seismic displacement applied to the QSD, the hydrodynamic sloshing force that develops and interacts with the shell can decompose into two constituents. The first element is a convective force directly related to the fluid sloshing movement. The second is an impulsive force where the motion of the fluid has zero relative acceleration relative to the QSD shell. Consequently, the total hydrodynamic pressure applied to the inside of the QSD shell also has a correlating impulsive and convective component. The sloshing motion is a superposition of few eigenmodes of the fluid motion. In general, each eigenmode generates a hydrodynamic wall pressure of different distribution, but not all of these modes contribute to the development of a non-zero horizontal force on the tank. The eigenmodes, responsible for the generation of a nonzero horizontal hydrodynamic force, influence the horizontal motion of the tank structure. These are few that exhibit free-surface antisymmetric to a plane parallel to the tank axis of symmetry. The convective masses, M_{cn}, are related to the sloshing modes $n = 1 \ldots$ to ∞. This and the impulsive mass, MI, are related via the principle of conservation of mass where n varies from 1 to 7 for the various sections of the tank (Tota-Maharaj and Ramroop 2020) as follows:

$$M = M_1 + \sum_{n=1} M_{Cn_i} + M_{cn}, \tag{1}$$

where M stands for the entire liquid mass. The total horizontal hydrodynamic force, F, applied on the tank due to the liquid motion is:

$$F(t) = M_1 \ddot{x}(t) - \sum_{i=1}^{7} M_{Cn_i} \omega_{Cn_i}^2 u_{Cn_i}(t) - M_{Cn} \omega_{Cn}^2 u_{cn}(t), \tag{2}$$

where $x(t)$ is the acceleration of the tank structure and $u_{cni}(t)$, $u_{cn}(t)$ is the response of a Single Degree of Freedom (SDOF) system, with frequency ω_{Cni}, ω_{Cni}, which is computed as a forcing input to the acceleration of the tank. The liquid in mass of the tank is modelled as Multiple Degrees of Freedom (MDOF) system since the liquid behaves as an MDOF oscillator. Therefore, the convective mass M_{Cn} of each sloshing mode is equal to an effective modal mass computed,

$$M_{Cn_i} = \frac{(L_{Cn_i})^2}{M_{n_i}}, \tag{3}$$

where:

$$M_n = \{\phi\}_n^T [M] \{\phi\}_n \tag{4}$$

is the generalised mass of eigenmode $n = 7$, and

$$L_{Cn} = \{\phi\}_n^T [M] \{I\} \tag{5}$$

with $\{L\}$ being the unit vector in the direction of the seismic excitation. In addition, the impulsive and convective parts of the fluid, the total hydrodynamic force can also be divided into an axisymmetric part, associated with the axisymmetric eigenmodes of the fluid motion which do not contribute to the total horizontal force:

$$p(\phi,\ \varphi,\ t) = p_I(\phi,\ \varphi,\ t) + \sum_{i=1}^{7} p_{Cn_i}(\phi,\ \varphi,\ t) + p_{Am}(\phi,\ \varphi,\ t), \tag{6}$$

where ϕ and φ are the azimuths and meridian angles, respectively as shown in Figure 3, p_I is the impulsive pressure, p_{Cn} is the convective pressure due to sloshing mode n and p_{Am} is the axisymmetric pressure due to axisymmetric mode m. Hence the impulsive pressure is given by:

$$p_I(\phi,\ \varphi,\ t) = C_1(\phi)\rho R(\phi)\cos(\varphi)\ddot{x}(t) \tag{7}$$

and convective pressure:

$$p_{Cn_i}(\phi,\ \varphi,\ t) = C_{Cn_i}(\phi)\omega_{Cn_i}^2\rho R(\phi)\cos(\varphi)u_{Cn_i}(t) \tag{8}$$

for each sloshing mode with C_i and C_{ni} being dimensionless pressure profile functions which depend on the tank fill height. The computation of CC_i and C_{ni} is based on a series of dynamic mode superposition analyses. Thus, for any fill height, the response of the fluid-structure concentrated mass model to an arbitrary seismic excitation is computed taking into consideration only the 8-th sloshing mode. The resulting hydrodynamic pressure distribution is equal to p_{cn} therefore, the profile functions C_{ni} can be computed using equation (8). Thereafter, a time domain simulation is performed, based on the same seismic excitation as in the dynamic mode superposition analysis, and the total hydrodynamic pressure distribution p is obtained.

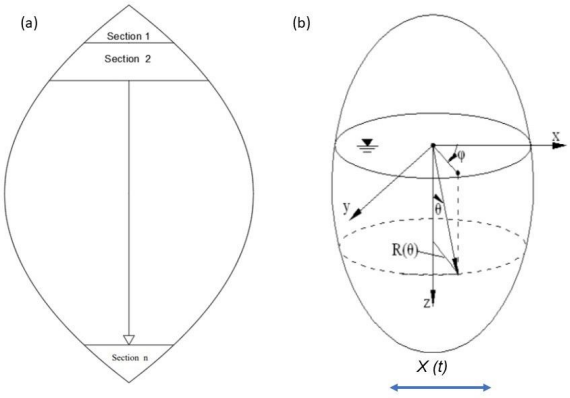

Fig. 3. (a) Sections of the QSD (n = 1 to 8) where Section 1 is the top of the tank and Section 8 is the base. (b) The coordinate system for axisymmetric components

For each sloshing mode, the stress components are calculated by dividing the respective forces by the shell thickness, Hence,

$$\sigma_{\theta j} = \frac{F_{\theta j}}{t_j} \tag{9}$$

and

$$\sigma_{\theta j} = \frac{F_{\varphi j}}{t_j} \tag{10}$$

where

$$F_{\theta j} = p \times \sin(\varphi) \tag{11}$$

and

$$F_{\varphi j} = p \times \cos(\varphi) \tag{12}$$

2.2. Smooth-Particle Hydrodynamic (SPH) – Finite Element Analysis (FEA) Model

The Smooth-Particle Hydrodynamic (SPH) procedure can account for hydrodynamics intricacies whose arrangement appears as a Partial Differential Equations (PDE) for field variables such as density, velocity and energy. Acquiring expository solutions for such an arrangement of PDEs is not frequently conceivable, aside from not very many straightforward cases. For numerical arrangements, one needs first to discretize the problem area where the PDEs are characterised so that the technique can give an estimate to the estimations of the field capacities and their derivatives at any point. The function approximation is then applied to the PDEs to create an arrangement of ODEs in a discretized form with respect only to time. This arrangement of discretized ODE can then be solved utilising one of the standard integration procedures of the

conventional FDM. The SPH formulation consists of two essential steps where the first step relating to the kernel approximation of field equations and the other relating to the particle approximation of the equation. During the first step of the SPH formulation in finite element analysis, integration of an arbitrary equation and smoothing kernel equation produces an integral representation of the kernel approximation of the SPH function. The integral representation of this function is computed based on nearby interacting particles, which then results in the particle approximation of the SPH function of a discrete particle within the model. In this project the combination of SPH and FE methods was used in one numerical model, whereby the SPH was used to discretise the volume of wastewater in the sludge digesters and FEM was used to discretise the structure of the walls. The code was developed by the authors and the SPH and FE combination was applied within the numerical model. As explained by Liu and Liu (2009), the kernel approximation of a function $f(x)$ is illustrated as Equation (13).

$$< f(x) >= \int_{\Omega}^{n} f(x')W(x - x', h)dx \tag{13}$$

where f is the function of the three-dimensional position vector x, Ω is the volume of the integral that contains x, W is the smoothing kernel function, x is a three-dimensional position vector. Johnson et al (1996) used the following quadratic smoothing kernel function as illustrated in Equation (13) to simulate the high-velocity impact problem.

$$W(R, h) = \alpha_d \left(\frac{3}{16} R^2 - \frac{3}{16} R + \frac{3}{4} \right), \tag{14}$$

where R is the relative distance between two particles at points x and $x' = R = r/h = |x - x'|/h$, r is the distance between the two points, α_d denotes the space dimension and is equal to one, two or three.

Conventional buildings in the Caribbean have a fixed base, whereas the structural and non-structural damages to the infrastructure substantially decrease as a result of base isolation applications. The base isolation system separates the structure from its foundation and primarily moves the natural frequency of the structure away from the dominant frequency range of the excitation via its low stiffness relative to that of the upper structure.

3. Results

3.1. First Principles Model with Shell Forces

The forces developed in the shell are the hoop or circumferential force, N_θ and the meridional force, N_φ. These forces were developed as ground acceleration amplitudes stemming from the simulated earthquake in the study. Upon comparing figures Figure 4a, 4b and Figure 5a and 5b it can be seen that the general shape of the change in the

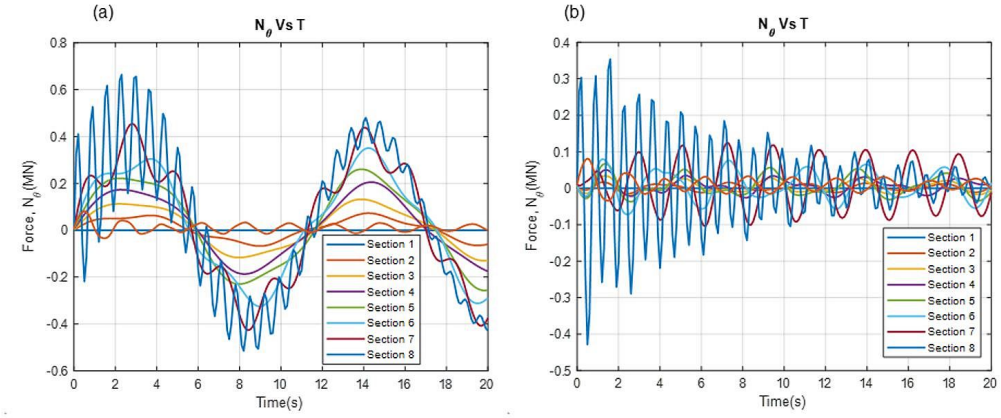

Fig. 4. Circumferential hoop force N_θ in QSD shell, for various sections at 5Hz for (a) Fixed base QSD and (b) Base-isolated QSD

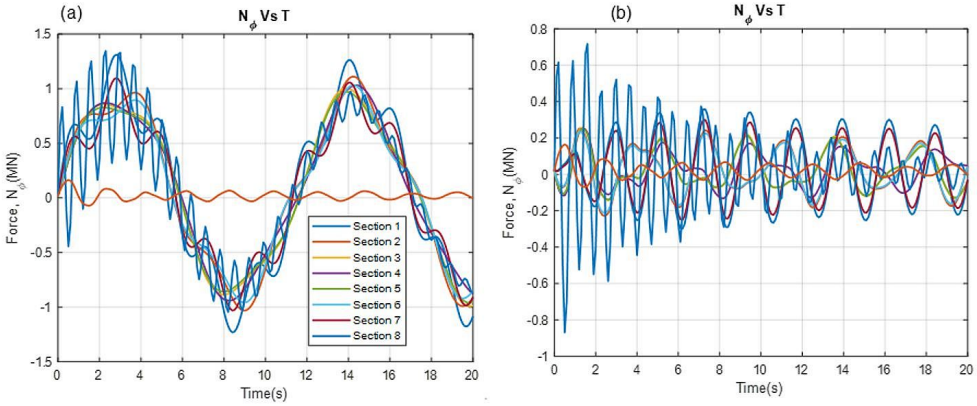

Fig. 5. Meridional force N_φ in QSD shell, for various sections at 5Hz for (a) Fixed base QSD and (b) Base-isolated QSD

forces follows the overall shape of the input frequency. Although the circumferential shell forces are almost similar, highest circumferential shell forces occur towards the lowest sections of the QSD (sections 7 and 8) while the highest meridional forces also occur in these sections. The highest N_φ values are attributed to the hydrostatic forces that occur in that region. The angular surface movement provides for an increase in meridional force at higher sections. Since the fluid becomes uneven at this section, the circumferential force is translated throughout the region; accordingly, the forces are analogous to those of the lower midsection. Overall, the N_φ is higher than the N_θ by 48.2%.

The N_θ and N_φ developed due to oscillations from the base isolated model, follow the same mechanical principles as those discussed for the fixed system. The difference is that the period for the frequency is only about 0.2 seconds and follows the

general shape of the displacement-bearing plot. The stresses, which were developed by Equations 9–10, take into account the mechanical properties of the material as well as the cross-sectional thickness at the section where the stress is measured. In Figure 6(a) and Figure 6(b) the maximum N_θ and N_φ both occur at the base (section 8). It is noticed that section 2 displays some increase in hoop stress. This corresponds to the angular displacement occurring at the free surface of the liquid during the excitation. The base isolated model shows a 10.2% reduction in circumferential stress after the transient behaviour has normalised. The meridional stresses are highest only in the base section of the QSD (Fig. 7). This attributed to both the hydrostatic pressure at the base as well as the axial shell loads due to gravity.

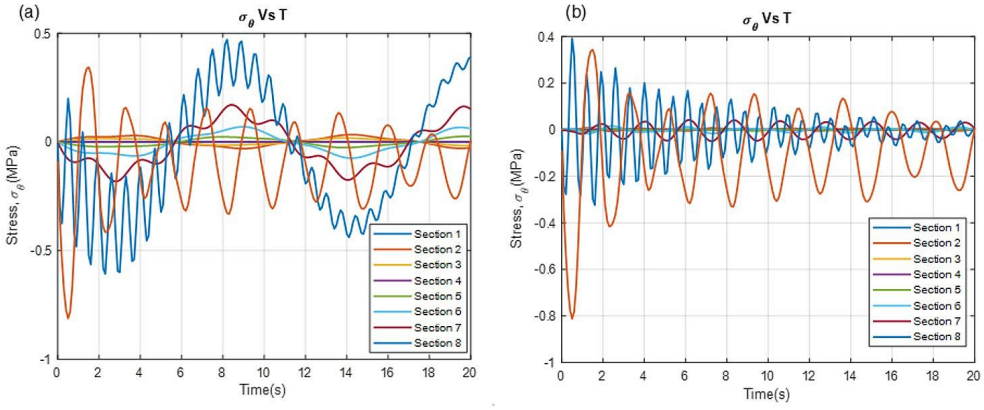

Fig. 6. Circumferential hoop force σ_θ in QSD shell, for various sections at 5Hz for (a) Fixed base QSD and (b) Base-isolated QSD

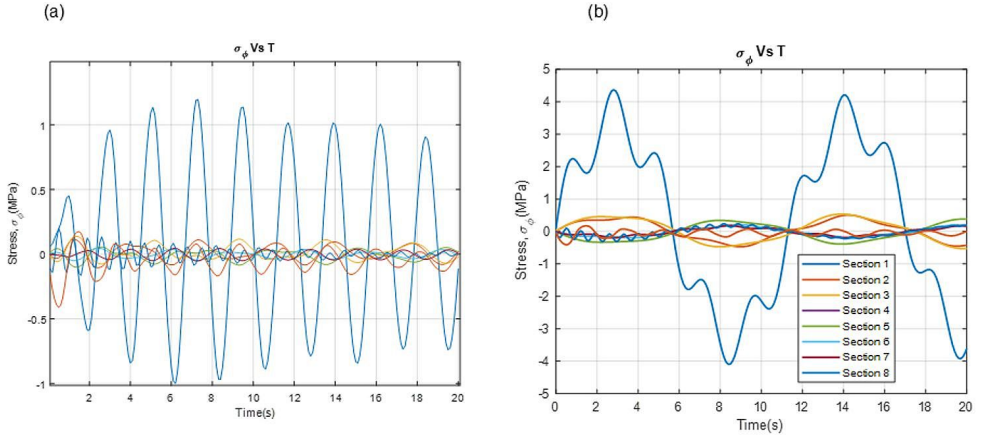

Fig. 7. Meridional force σ_φ in QSD shell, for various sections at 5Hz for (a) Fixed base QSD and (b) Base-isolated QSD

3.2. QSD Simulations under Varying Wastewater Fill Conditions

Simulations were conducted simultaneously on the QSD outlined in Table 2. Each simulation had the same parameters except for the fill levels. Five (5) fill levels of 10%, 25%, 50%, 75%, and 90% were each assigned to a separate model respectively. The peak impulsive displacements varied between each model. The highest impulsive displacement occurred in the QSD with the lowest fill level (10% fill- level 1) (see Figure 8). This occurred for both the rigid base and isolated base models because of the smaller volumetric mass coupled with a lighter convective mass. By contrast, the lowest impulsive displacement is at 90% fill. Both plots show that at 3.1 metres from the base of the QSD is where the maximum peak displacement occurs. The base and at heights between 10 and 20 metres have low displacements. The base is rigidly fixed hence the displacement will be small.

Table 2. Quadric-Surfaced Sludge Digesters (QSD) Design Parameters

Design Parameter	Value
Height	25 m
Diameter	12.5 m
Minimum Shell Thickness	1 m
Maximum Shell Thickness	2 m
Ground excitation (harmonic)	5 Hz
Fill Level	50%

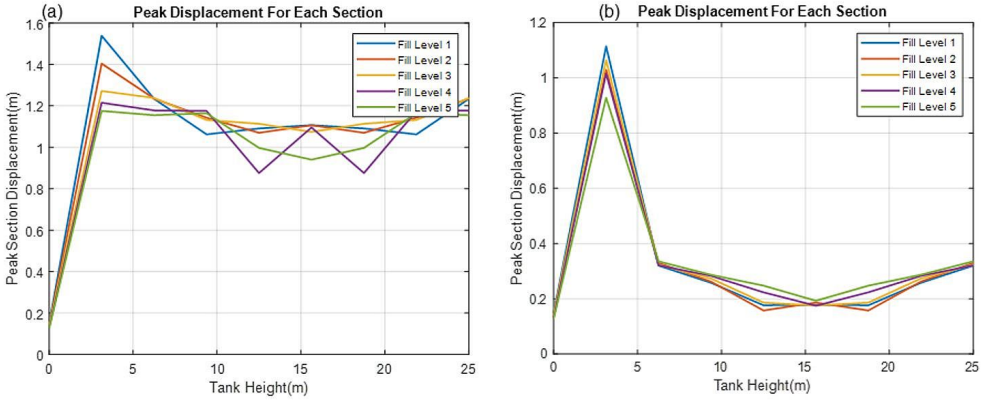

Fig. 8. Comparison of peak impulsive displacement of fluid in QSD, for various fill levels at 5Hz for (a) Fixed base QSD and (b) Base-isolated QSD (Level 1–10% fill, Level 2–25% fill, Level 3–50% fill, Level 4–75% fill, Level 5–90% fill)

On comparing the peak hoop stresses for the different fill levels, it was found that for the rigid-base model the stress variation was almost negligible (Figure 9). The

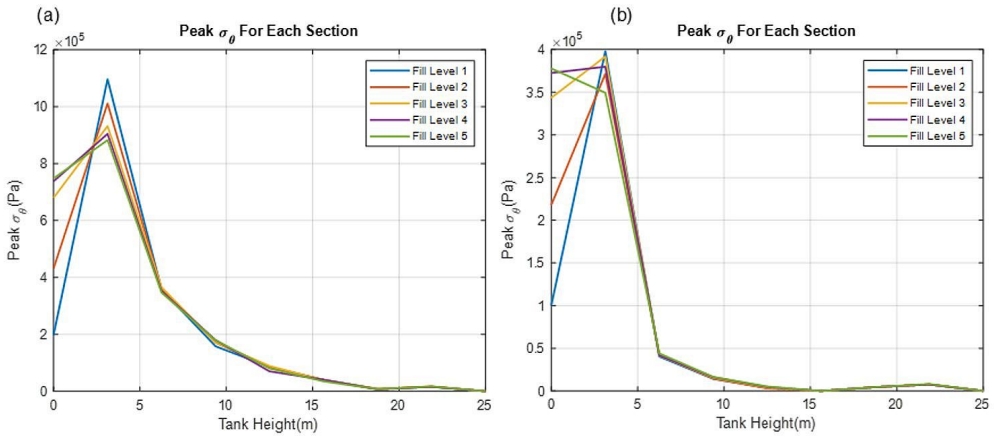

Fig. 9. Comparison of peak circumferential hoop stress σ_θ in QSD shell, for various fill levels at 5Hz for (a) Fixed base QSD and (b) Base-isolated QSD (Level 1–10% fill, Level 2–25% fill, Level 3–50% fill, Level 4–75% fill, Level 5–90% fill)

base isolated QSD displayed a reduction of 36.3%. The peak meridional displayed a similar relationship; however, the maximum stress was at the base (Figure 10).

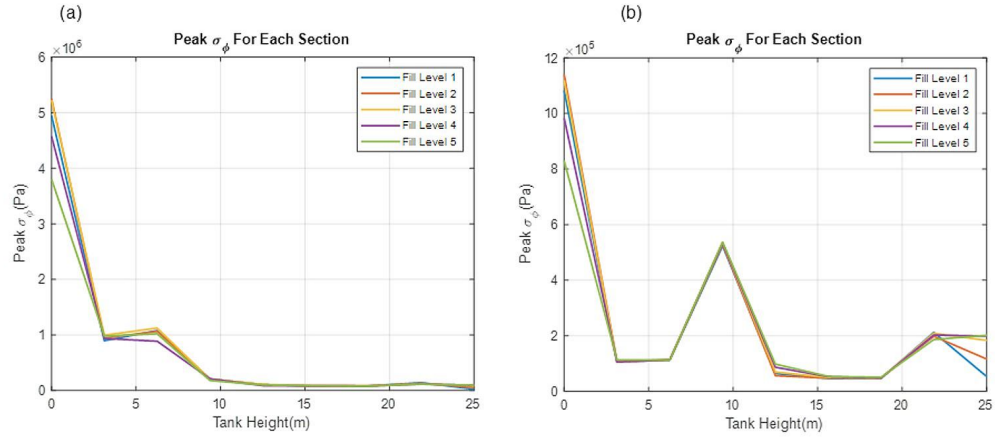

Fig. 10. Comparison of peak meridional hoop stress σ_θ in QSD shell, for various fill levels at 5Hz for (a) Fixed base QSD and (b) Base-isolated QSD (Level 1–10% fill, Level 2–25% fill, Level 3–50% fill, Level 4–75% fill, Level 5–90% fill)

3.3. Two-Dimensional (2-D) SPH-FEA Computational Models

The Two-Dimensional (2-D) analyses were grouped into two categories, the first was hydrostatically loaded and the second was dynamically loaded. 25 simulations were conducted for each load case (150 simulations total). The hydrostatic cases proved that the orthogonal stresses increased as the fill level increased (see Figure 11). This

stress was reduced as the shell thickness increased. Comparing this with the dynamic cases, the hydrostatic levels produced the most internal stresses in the shell structure.

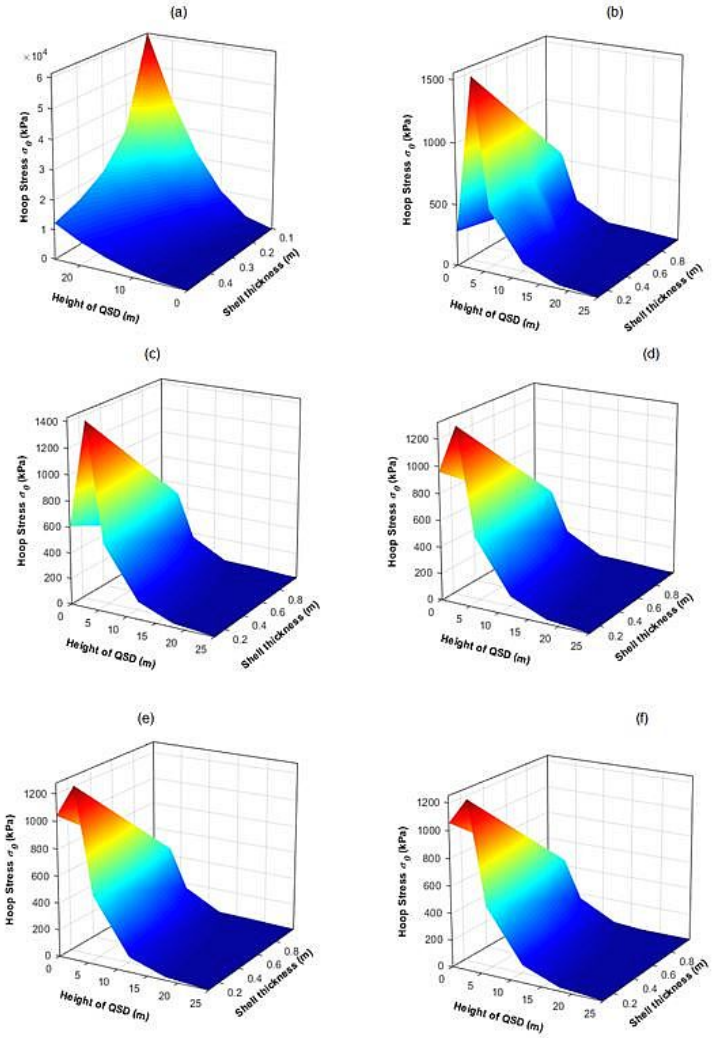

Fig. 11. Surface plot results for meridional hoop stress for analyses with varying wall thicknesses for 25 m tall QSD for: (a) 90% fill – hydrostatic case, (b) 10% – fill dynamic case (c) 25% fill – dynamic case, (d) 50% fill – dynamic case, (e) 75% fill – dynamic case. (f) 90% fill – dynamic case

The results produced by the 2D FEA analyses were in close agreement with those from the first principle analyses. There was a sharp increase in internal stresses at the 3.1-metre height. This confirms that the impulsive forces coupled with the hydrostatic forces produce an increase in this area. It's also quite noticeable that the lower fill lev-

els have higher stresses at this level. This is due to the convective force produced by the sloshing of the surface in this area the inverted frustum shape at this level, encourages the hydrodynamic movement of the surface to produce a significant sloshing mode. As the fill level increases after the equator, the frustum is inverted and the shape dampens the sloshing at the higher levels. The plan area of the liquid level also decreases which reduces the impulsive force. It was also noted that the impulsive force was gradually replaced with the hydrostatic pressure at the 3.1 m height. To properly assess the data generated by the 125 dynamic cases, a multiple Analysis of Variance (ANOVA) was carried out by only considering the main effects, 2-way and 3-way interactions of the variables vertical distance, shell thickness, maximum QSD height, and fill levels on the variable stress. The results show that model was significant (p-*value* < 0.05) in determining the stress. On examination of the separate effects on the dependent variable stress, it was observed that the main effects of height, fill, vertical distance and shell thickness were also seen to be significant factors (p-*value* < 0.05) for stress. On examination of the two-way interactions, it can be deduced that two-way interactions between distance and thickness, distance and height, distance and fill, thickness and fill and height and fill were also significant factors in assessing the stress. However, the interaction between thickness and height was found to be insignificant (p-*value* $= 0.706$).

The 3-way interaction between distance, thickness and fill were also found to have a significant effect on the variable stress (p-*value* < 0.05). The 3-way interaction between distance, thickness and fill were also found to have a significant effect on the variable stress (p-*value* < 0.05). The shell thickness did have a significant effect on the stress across the different fill levels. As the thickness increased, the stress decreased. There was no significant effect of fill at higher thicknesses on the stress variable. The interaction effect of thickness and fill was significant and was a medium effect (Partial Eta-Squared = 0.617). The vertical distance can be seen to have a significant effect on stress at lower values of the thickness. Both the main effect and interaction effect of distance and thickness was significant with the interaction effect being a strong effect (Partial Eta-Squared = 0.988). The analysis revealed that the main effect for height was significant. There was a drastic increase in stress at the 75% fill level after a height of 20. However, at smaller heights, there was no significant effect on stress due to the fill level. The interaction effect between height and fill was shown to be weak (Partial Eta-squared = 0.268). The main effect on stress was also observed to be a weak effect (Partial Eta-Squared = 0.196). Distance was seen to have a significant effect on stress especially at higher values (p-*value* < 0.05). There was a large increase in stress at the greater distances for the fill value of 75%. The interaction effect between distance and fill was observed to be a strong effect (Partial Eta-Squared = 0.951). Although the interaction effect of distance and height was shown to be significant (p-*value* < 0.05), the effect was a weak one (Partial Eta-Squared = 0.295). There was no significant increase in stress at different distances for the varying heights of 1, 5 and 10 m. However, a sharp increase was observed for larger distances at heights of 20 and 25 m.

3.4. Computational Models for 3-Dimensional (3-D) SPH FEA

The 3-Dimesional 3-D FEA SPH simulation was conducted for the 25-metre model. This 6 degree-of-freedom model utilised the Kobe, Takatori 1995 time-history data as the ground motion. 50% fill level was selected since this produced the most significant convective force at the surface. The analysis utilized parallelization with 16 CPU cores (total of 32 threads). The run time was 419 hours. The results from the computational models were in good agreement with those from the first principles model as well as the 2-D FEA models. Figures 12 and 13 show the hoop stresses and the meridional stresses respectively.

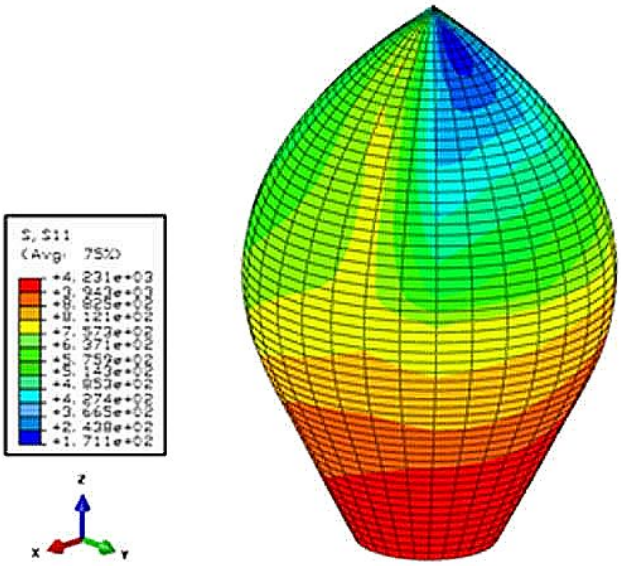

Fig. 12. 3D FEA SPH output showing S11 stresses

The results show that hydrostatic pressure coupled with the convective surface pressure impacted mainly on the lower third of the shell. Sloshing forces did not have a significant impact on the upper portions of the QSD. Failure can occur if the Von Mises stress computed is more than the material stress limit. In high magnitude events, high particle velocity would induce high pressures with would interact with the retaining surface and induce high stress which would create small or large displacements and may be in areas that local stress exceeds the material stress and failure occurs. The von Mises stresses (see Figure 14) show that the 3D printed FDM ABS can be a viable option for the shell of the QSD since it is within range of the material property.

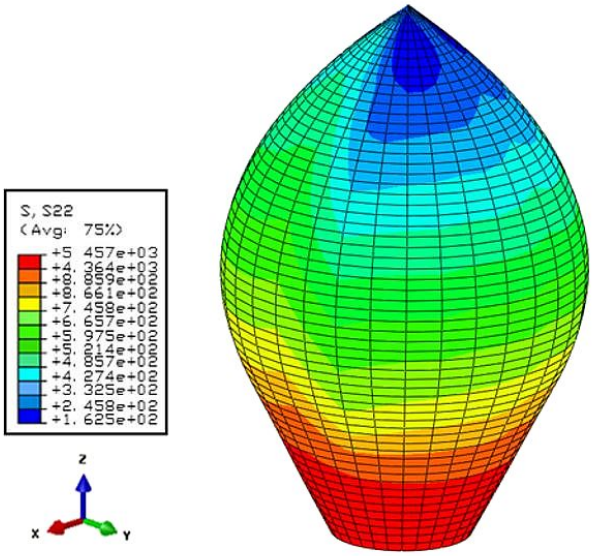

Fig. 13. 3D FEA SPH output showing S22 stresses

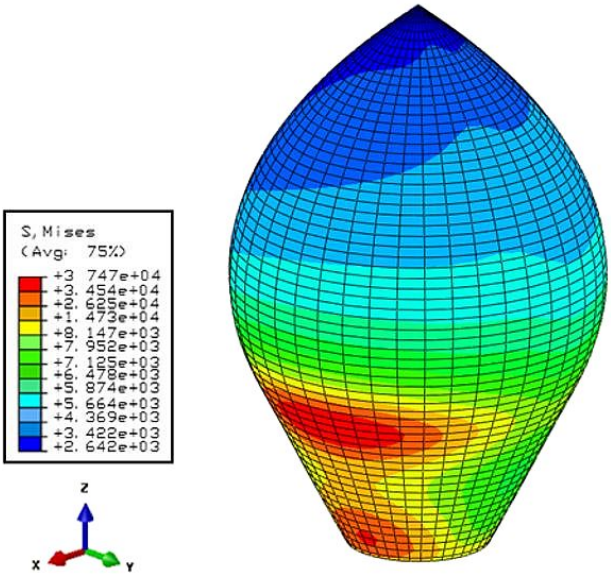

Fig. 14. 3D FEA SPH output showing Von Mises stresses

4. Conclusions

Three groups of analyses were conducted by Smoothed Particle Hydrodynamics (SPH)-Finite Element (FE) Methods for computing the orthogonal stresses in the shell

of the Quadratic-Surface Sludge Digesters (QSD). The 3-way interaction between distance (sections across the tank for $n = 1$ to 7), thickness and fill levels (Level 1 – 10% fill, Level 2 – 25% fill, Level 3 – 50% fill, Level 4 – 75% fill, Level 5 – 90%) of the QSD were analysed statistically based on 125 dynamic cases and were found to have significant impacts on the variable stresses ($p\text{-}value < 0.05$). The first-principles numerical models ran reasonably quickly, and many simulations were made during the study. The results showed that they were within the range of 5.34% to 7.2% to 2D FEA simulation results. The 3D FEA simulations were within the range of 8.3% to 9.2% to results from the MATLAB time-history models. This is a good indicator that the first principles numerical models are an excellent timesaving method to predict the behaviour of the QSD under seismic excitation. Upon examining the criteria for the design, the analysis of the results for the 2D FEA simulations showed that the fill height is not a significant variable with sloshing, however, the 3D FEA results showed that the hydrostatic pressure is a significant variable. With the maximum tensile stress of the 3D-printed ABS being equal to 24.4 MPa, the overall maximum stress was 5.45 MPa, so this material application can be a viable option for the use of QSD construction.

Acknowledgments

The authors would like to thank Dr Keerthan Poologanathan (Associate Professor in Structural Engineering) from Northumbria University for his valuable comments and suggestions to this research project. This work was supported by the International Water Security Network (IWSN), Aston University, Birmingham, UK, The University of West of England (UWE Bristol) and The University of Trinidad and Tobago (UTT).

References

Abramson H. (1967) *The dynamic behavior of liquids in moving containers, with applications to space vehicle technology*, Washington: Govt. Pr.

Hutchinson A. (2010) Rain Water Harvesting – Case Studies from the Barbados Experience, *Conference Proceedings*, Caribbean Waste Water Association Conference, Grenada. 1–14

Ibrahim R. (2006) *Liquid sloshing dynamics*, Cambridge, Cambridge University Press.

Johnson G., Stryk R., Beissel S. (1996) SPH for high velocity impact computations, *Computer Methods in Applied Mechanics and Engineering*, **139** (1–4), 347–373.

Liu G., Liu M. (2009) *Smoothed Particle Hydrodynamics*, Singapore: World Scientific.

Sumner I. E. (1966) *Experimental investigation of stability boundaries for planar and nonplanar sloshing in spherical tanks*, National Aeronautics and Space Administration.

Tota-Maharaj K., Ramroop N. (2020) Numerical modelling of Quadric-Surfaced Sludge Digesters (QSD) within wastewater infrastructure using 3D printing techniques *Institute of Water Journal*, **4**, 25–31.

Zingoni A. (2001) Stresses and deformations in egg-shaped sludge digesters: Membrane effects, *Engineering Structures*, **23** (11), 1365–1372.